Asymmetry in the analogous spin–isospin-flip excitations of the $[J^\pi, T] = [2^+, 1]_1$ and $[2^+, 1]_2$ states in ${}^{14}_{6}C_8$, ${}^{14}_{7}N_7$, and ${}^{14}_{8}O_6$ from the $[1^+, 0]_1$ ground state of ${}^{14}N$

H. Fujita,[1,2,*] Y. Fujita,[1,2] P. Adsley,[3,4] J. W. Brümmer,[3] A. Fujimoto,[5] D. Houngbo,[6] M. Kohne,[3] K. C. W. Li,[3] P. Z. Mabika,[7] A. Negret,[8] R. Neveling,[4] P. Papka,[3,4] L. Pellegri,[4,9] F. D. Smit,[4] and S. Triambak[10]

[1]Research Center for Nuclear Physics, Osaka University, Ibaraki, Osaka 567-0047, Japan
[2]Department of Physics, Osaka University, Toyonaka, Osaka 560-0043, Japan
[3]Department of Physics, University of Stellenbosch, Matieland 7602, South Africa
[4]iThemba LABS, P. O. Box 722, Somerset West 7129, South Africa
[5]Faculty of Engineering, Osaka Institute of Technology, Osaka, Osaka 535-8585, Japan
[6]SCK-CEN, Boeretang 200, 2400 Mol, Belgium
[7]Department of Physics and Astronomy, University of the Western Cape, Robert Sobukwe Road, Bellville 7535, South Africa
[8]Horia Hulubei National Institute of Physics and Nuclear Engineering (IFIN-HH), R-76900 Bucharest, Romania
[9]School of Physics, University of the Witwatersrand, Johannesburg 2050, South Africa
[10]Department of Physics, University of the Western Cape, Robert Sobukwe Road, Bellville 7535, South Africa

(Received 9 September 2024; accepted 23 December 2024; published 14 January 2025)

This study investigated the asymmetry among the analogous spin-isospin-flip transition strengths from the $[J^\pi, T] = [1^+, 0]_1$ ground state of ${}^{14}N$ to the $[2^+, 1]_1$ and $[2^+, 1]_2$ states in the $A = 14$ nuclei ${}^{14}_{6}C_8$, ${}^{14}_{7}N_7$, and ${}^{14}_{8}O_6$. The reduced transition strengths for the excited states in ${}^{14}N$, denoted by $B(\mathrm{GT}^0)$, were obtained via a ${}^{14}N(p, p')$ experiment at $E_p = 200$ MeV performed at iThemba LABS, South Africa. The $B(\mathrm{GT}^0)$ values obtained for the $[2^+, 1]_1$ and $[2^+, 1]_2$ states in ${}^{14}N$ were compared with the $B(\mathrm{GT}^+)$ and $B(\mathrm{GT}^-)$ values for the analogous states in ${}^{14}C$ and ${}^{14}O$, which are available from the charge-exchange reaction measurements. Based on the simple two-state model, the off-diagonal matrix elements of the nuclear Hamiltonians $\langle H_C^+\rangle$ and $\langle H_C^-\rangle$ for ${}^{14}C$ and ${}^{14}O$, respectively, were deduced. The obtained $\langle H_C^\pm\rangle$ values are roughly proportional to the T_z values of the respective nuclei.

DOI: 10.1103/PhysRevC.111.014317

I. INTRODUCTION

Assuming that isospin T is a good quantum number, it is expected that isobars will commonly have states with the same properties, except for their third component of isospin, $T_z = (N - Z)/2$. These states are known as isospin-analogous states. One transition and another from the same initial state or its analogous state to the same final state or its analogous state are known as analogous transitions.

Example of analogous transitions are Gamow-Teller$^+$ (GT^+), isovector (IV) spin-$M1$ [1,2], and GT^- transitions, which are spin-isospin-flip processes characterized by $\Delta T_z = +1$, 0, and -1, respectively. For studying GT^+ and GT^- transitions, it is known that the (n, p)- and (p, n)-type charge-exchange (CE) reactions performed at an intermediate incident energy and at a scattering angle of 0° are suitable [1,3–5]. Similarly to the $\mathrm{GT}^\pm$ transitions, proton inelastic scattering is suitable for studying IV spin-$M1$ transition [1,2,6–8]. This is because proportional relationships exist between the cross sections of the respective reactions and the reduced strengths of GT^+, IV spin-$M1$, and GT^- transitions, which are denoted by $B(\mathrm{GT}^+)$, $B(\mathrm{GT}^0)$, and $B(\mathrm{GT}^-)$, respectively.

*Contact author: hfujita@rcnp.osaka-u.ac.jp

It is known that isospin is a reasonably good quantum number in nuclei. However, it is not perfect due to the Coulomb interaction, or more generally, the charge-asymmetric interaction [1]. To examine the purity of isospin, one can study isospin mixing using the CE reaction. For example, using the high resolution ${}^{56}\mathrm{Fe}({}^3\mathrm{He}, t)\,{}^{56}\mathrm{Co}$ reaction measurements at 140 MeV/nucleon and 100 MeV/nucleon, the isospin mixing between the two nearby 0^+ states in ${}^{56}\mathrm{Co}$, namely the isobaric analog state (IAS) at the excitation energy (E_x) of 3.599 MeV and the nearby 0^+ state at 3.527 MeV with the nominal isospin $T = 2$ and 1, respectively, was investigated [9]. The nuclear Hamiltonian's off-diagonal term connecting these states, $\langle H_C\rangle$ of 32.3(5) keV was obtained. Similar results have also been reported in studies at lower incident energies [10,11].

The charge-asymmetric interaction also affects the isospin symmetry between analogous states. Isospin symmetries for $A = 41$ and 37 nuclei have been studied by comparing the analogous GT^- and GT^+ transitions of $T_z = +3/2 \to +1/2$ and $T_z = -3/2 \to -1/2$, respectively [12,13]. In Ref. [12], the GT^- transitions excited by the ${}^{41}_{19}\mathrm{K}_{22}({}^3\mathrm{He}, t)\,{}^{41}_{20}\mathrm{Ca}_{21}$ reaction at 140 MeV/nucleon and the mirror GT^+ transitions investigated by the β^+ decay from ${}^{41}_{22}\mathrm{Ti}_{19}$ to ${}^{41}_{21}\mathrm{Sc}_{20}$ are compared up to an excitation energy E_x of 8 MeV. A one-to-one correspondence was found up to 6.2 MeV due to the similar $\mathrm{GT}^\pm$ strength distributions. For the doublet states at approximately 5 MeV, which exhibit significant asymmetry, an estimate of the off-diagonal term of the nuclear Hamiltonian $\langle H_C \rangle$ of 8 keV was obtained.

In Ref. [13], a similar comparison of the analogous GT$^{\pm}$ transitions studied by the $^{37}_{17}\mathrm{Cl}_{20}(^{3}\mathrm{He}, t)\,^{37}_{18}\mathrm{Ar}_{19}$ reaction at 140 MeV/nucleon and the β^{+} decay from $^{37}_{20}\mathrm{Ca}_{17}$ to $^{37}_{19}\mathrm{K}_{18}$ was performed up to 8.6 MeV. A one-to-one correspondence was found up to 5.1 MeV. The overall distributions are similar, but the fine structures may not be in agreement.

These studies on the $A = 41$ and 37 nuclei [12,13] revealed that one-to-one correspondences up to 5–6 MeV were found among these nuclei. This suggests that the charge-asymmetric interaction may have contributed to the lack of symmetry in the highly excited regions. However, the excitation energy regions that can be compared are limited by the threshold energies for the β decays. In addition, high level densities of the odd-mass nuclei prevent a level-by-level comparison. By comparing the (n, p)- and (p, n)-type CE reactions on the even-mass nuclei with lower level density, one can study the isospin symmetry between the analogous GT$^{\pm}$ transitions without suffering from high level densities and from the threshold energy of the β decay.

In Fig. 1, the GT$^{\pm}$ transitions from the ^{14}N ground state to the states in ^{14}C and ^{14}O are illustrated. The analogous IV spin-$M1$ transitions to the excited states in ^{14}N are also shown. In Refs. [14–16], the isospin symmetry of the analogous GT^{+} and GT^{-} transitions was investigated by means of the CE $^{14}_{7}\mathrm{N}_{7}(d, {}^{2}\mathrm{He})\,^{14}_{6}\mathrm{C}_{8}$ and $^{14}_{7}\mathrm{N}_{7}(^{3}\mathrm{He}, t)\,^{14}_{8}\mathrm{O}_{6}$ reaction measurements. Between the two prominent $[J^{\pi}, T] = [2^{+}, 1]_1$ and $[2^{+}, 1]_2$ states at the E_x values of 7.01 and 8.32 MeV in ^{14}C and their analogous $[2^{+}, 1]_1$ and $[2^{+}, 1]_2$ states at 6.61 and 7.78 MeV in ^{14}O, the asymmetric $B(\mathrm{GT}^{\pm})$ values were found [16]. As indicated in Fig. 1, in this paper, the $[2^{+}, 1]_1$ and $[2^{+}, 1]_2$ states in ^{14}C and ^{14}O are referred to as A_{+} and B_{+} and A_{-} and B_{-}, respectively.

By also considering the $B(\mathrm{GT}^{0})$ values for the analogous IV spin-$M1$ transitions to the $[2^{+}, 1]_1$ and $[2^{+}, 1]_2$ states at 9.17 and 10.43 MeV in ^{14}N, we investigate the isospin asymmetry among the complete set of analogous spin-isospin-flip transitions (see Fig. 1). Similarly to $A_{\pm}$ and $B_{\pm}$, the $[2^{+}, 1]_1$ and $[2^{+}, 1]_2$ states in ^{14}N are referred to as A_0 and B_0, respectively. Using a high-energy-resolution $^{14}\mathrm{N}(p, p')$ experiment at an incident proton energy of 200 MeV and at forward scattering angles including 0°, we derive the $B(\mathrm{GT}^{0})$ values for the A_0 and B_0 states and the other excited states. From the comparison of the $B(\mathrm{GT}^{0})$ and $B(\mathrm{GT}^{+})$ values, the off-diagonal term of the nuclear Hamiltonian $\langle H_C^{+} \rangle$ for ^{14}C is derived, which causes the asymmetry of the A_{+} and B_{+} states in ^{14}C relative to their analogous states in ^{14}N. From the comparison of $B(\mathrm{GT}^{0})$ and $B(\mathrm{GT}^{-})$ values, the similar off-diagonal term $\langle H_C^{-} \rangle$ is also derived for ^{14}O.

II. SPIN-ISOSPIN-FLIP TRANSITION

The GT$^{\pm}$ transitions, caused by the $\boldsymbol{\sigma}\tau^{\pm}$ operators, are spin-isospin-flip ($\Delta S = 1$ and $\Delta T = 1$) processes in the $\Delta T_z = \pm 1$ directions without orbital angular momentum transfer ($\Delta L = 0$). Hence, such transitions exhibit an IV nature and possess a ΔJ^{π} value of 1^{+}. The reduced transition strengths $B(\mathrm{GT}^{\pm})$ are defined by [1]:

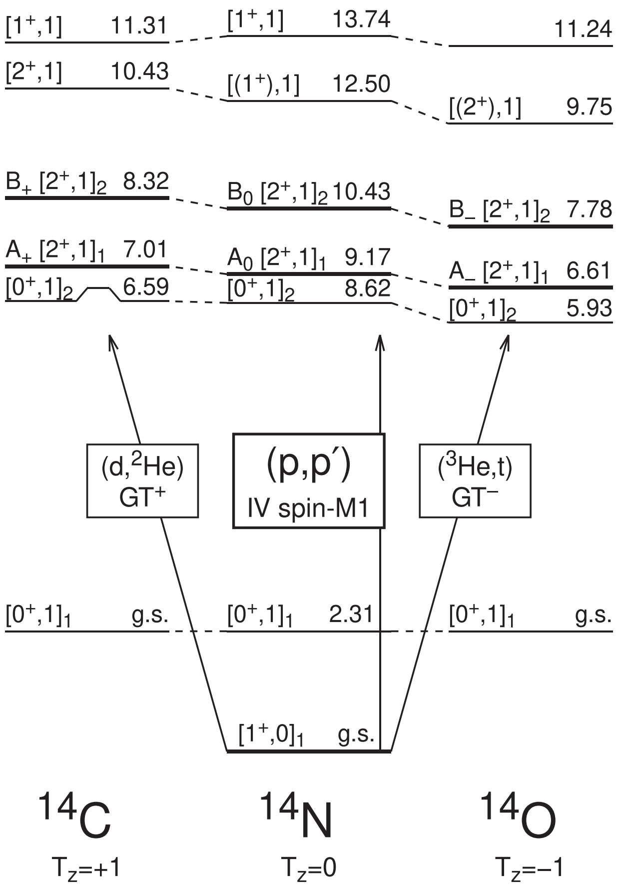

FIG. 1. Schematic view of the analogous GT^{+}, IV spin-$M1$, and GT^{-} transitions from the ^{14}N ground state with $[J^{\pi}, T] = [1^{+}, 0]_1$ to the excited states with isospin $T = 1$. The $[0^{+}, 1]_1$ ground states of ^{14}C and ^{14}O are aligned with their analogous state in ^{14}N, i.e., the $[0^{+}, 1]_1$ state at 2.31 MeV, so as to show relative excitation energies from these states. The E_x values of the excited states in ^{14}O are taken from Ref. [14].

$$B(\mathrm{GT}^{\pm}) = \frac{1}{2J_i + 1} |\langle f \,|\, \boldsymbol{\sigma}\tau^{\pm} \,|\, i \rangle|^2 = \frac{1}{2}\frac{1}{2J_i + 1}\frac{C^2_{\mathrm{GT}\pm}}{2T_f + 1}|M^{\pm}_{\sigma\tau}|^2, \tag{1}$$

where $C_{\mathrm{GT}\pm}$ denote the isospin Clebsch-Gordan (CG) coefficients for the GT$^{\pm}$ transitions and $M^{\pm}_{\sigma\tau}$ denote the $\boldsymbol{\sigma}\tau^{\pm}$ transition matrix elements. Starting from the ^{14}N ground state with isospin $T = 0$, the final states of GT$^{\pm}$ transitions have only $T = 1$ and thus the squared values of the CG coefficients, $C^2_{\mathrm{GT}\pm}$, are equal to 1.

For CE reactions performed at 0° and at intermediate incident energies, it is known that there is a good proportionality between the reaction cross sections at zero momentum transfer $q = 0$ and the $B(\mathrm{GT}^{\pm})$ values [1,4,5]:

$$\frac{d\sigma_{\mathrm{GT}\pm}}{d\Omega}(q = 0) = \hat{\sigma}_{\mathrm{GT}} B(\mathrm{GT}^{\pm}), \tag{2}$$

where $\hat{\sigma}_{\mathrm{GT}}$ is the GT unit cross section.

Proton inelastic scattering can also cause a $\Delta J^{\pi} = 1^{+}$ transition. This is referred to as a spin-$M1$ transition that does not change the N and Z values of the target nucleus ($\Delta T_z = 0$) and does not involve orbital angular momentum transfer ($\Delta L = 0$) [1,2].

In contrast to the GT$^{\pm}$ transitions, both the IV ($\Delta T = 1$) and the isoscalar (IS, $\Delta T = 0$) processes are allowed in the spin-$M1$ transition. Starting from the ground state of ^{14}N with an initial isospin of $T = 0$, states with $T = 0$ and $T = 1$ can be excited by IS and IV processes, respectively. The IV spin-$M1$ transition is mainly caused by the $\boldsymbol{\sigma}\tau^0$ operator and thus it has a spin-isospin-flip nature. As a consequence, such a transition is analogous to the GT$^{\pm}$ transitions.

The reduced IV spin-$M1$ transition strength, $B(\mathrm{GT}^0)$, is defined by [1,2]:

$$B(\mathrm{GT}^0) = \frac{1}{2J_i + 1}|\langle f \mid \boldsymbol{\sigma}\tau^0 \mid i\rangle|^2 = \frac{1}{2}\frac{1}{2J_i + 1}\frac{C_{M1}^2}{2T_f + 1}\left|M_{\sigma\tau}^0\right|^2, \tag{3}$$

where C_{M1} denotes the isospin CG coefficient for the IV spin-$M1$ transitions and $M_{\sigma\tau}^0$ denotes the $\boldsymbol{\sigma}\tau^0$ transition matrix element. As written above, the spin-$M1$ transitions from the ^{14}N ground state with $T = 0$ to the states with $T = 1$ are purely IV and thus the squared value of the CG coefficient, C_{M1}, is equal to 1.

In general, both the $M_{\sigma\tau}^{\pm}$ and $M_{\sigma\tau}^0$ terms of GT$^{\pm}$ and IV spin-$M1$ transitions exhibit quenching effects. The reduction is partly attributed to the meson exchange currents (MEC), which can affect GT$^{\pm}$ and IV spin-$M1$ transitions differently [1,2,17]. This effect is represented by the R_{MEC} ratio defined by

$$R_{\mathrm{MEC}} = \frac{\left|M_{\sigma\tau}^0\right|^2}{|M_{\sigma\tau}^{\pm}|^2}. \tag{4}$$

Taking the MEC contribution into consideration, Eq. (3) can be modified as

$$B(\mathrm{GT}^0) = \frac{1}{2}\frac{1}{2J_i + 1}\frac{C_{M1}^2}{2T_f + 1}\left|M_{\sigma\tau}^0{}'\right|^2, \tag{5}$$

where

$$\left|M_{\sigma\tau}^0{}'\right|^2 = \frac{\left|M_{\sigma\tau}^0\right|^2}{R_{\mathrm{MEC}}}. \tag{6}$$

Note that, the latest coupled-cluster calculation well reproduces the GT^{+} strength distribution measured by ^{14}O$(d,{}^2$He$)\,^{14}$N reaction without a phenomenological quenching factor [18]. This fact implies that the MEC effect in the $A = 14$ system is weak.

Proton inelastic scattering has been found to be a suitable method for studying the IV spin-$M1$ transitions, which are similar to the CE reactions used to study the GT$^{\pm}$ transitions [1,2]. At intermediate incident energies, it is known that there is a proportionality between the reaction cross sections at zero momentum transfer $q = 0$ and the $B(\mathrm{GT}^0)$ values [1,2,6–8]. Similarly to Eq. (2), the proportional relationship is expressed as

$$\frac{d\sigma_{M1}}{d\Omega}(q = 0) = \hat{\sigma}_{M1}B(\mathrm{GT}^0), \tag{7}$$

where $\hat{\sigma}_{M1}$ represents the unit cross section of the IV spin-$M1$ transition.

The proportional relationships shown by Eqs. (2) and (7) can be deteriorated by the incoherent $\Delta L = 2$ contribution and the coherent contribution mainly from the noncentral tensor ($T\tau$) interaction in nuclear reactions. The former, which is typically significantly weaker than the $\Delta L = 0$ component at 0°, can be estimated by comparing the angular distribution of the differential cross sections obtained from the measurements with those from the calculations for the $\Delta L = 0$ and $\Delta L = 2$ components. In Ref. [19], the effect of the latter was estimated through the ^{26}Mg(^{3}He, t) reaction at 140 MeV/nucleon. Uncertainty of the $B(\mathrm{GT}^-)$ values determined by Eq. (2) due to these non-GT transitions is estimated to be $\sim$10% for a transition with $B(\mathrm{GT}^-) = 0.1$ and decreases for the larger $B(\mathrm{GT}^-)$ values [19].

In this paper, we compare the analogous GT^{+}, IV spin-$M1$, and GT^{-} transition strengths from the ^{14}N ground state with isospin $T = 0$ to the states with $T = 1$ in ^{14}C, ^{14}N, and ^{14}O, respectively. In these cases, it is worth noting that all transitions are purely IV and the squared isospin CG coefficients, $C_{\mathrm{GT}\pm}^2$ and C_{M1}^2, are equal to 1. Assuming isospin symmetry and a constant R_{MEC} value, the analogous $M_{\sigma\tau}^{\pm}$ and $M_{\sigma\tau}^0{}'$ terms are identical and the analogous $B(\mathrm{GT}^{\pm})$ and $B(\mathrm{GT}^0)$ values are also identical [see Eqs. (1) and (5)]. Therefore, the differences between the analogous $B(\mathrm{GT}^{\pm})$ and $B(\mathrm{GT}^0)$ values can provide an insight into the asymmetry among the final states.

III. EXPERIMENT

In order to obtain the $B(\mathrm{GT}^0)$ values, the ^{14}N(p, p') experiment was performed at iThemba LABS, South Africa. A proton beam of 1–2 nA with an incident energy of $E_p =$ 200 MeV from the cyclotron was dispersively transported to realize the dispersion-matched conditions [20,21] for better energy resolution. As a self-supporting ^{14}N target, a commercially available melamine ($C_3H_6N_6$) resin with an areal density of $\sim$2 mg/cm^2 was used. To calibrate the absolute cross sections, the (p, p') data were also acquired with a pure melamine resin and a natural carbon foil with areal densities of 60 and 0.5 mg/cm^2, respectively. The procedure of the polymerization process of the pure melamine resin target is summarized in Appendix.

Inelastically scattered protons were momentum analyzed by the K600 magnetic spectrometer. The measurements were performed at several spectrometer angles between 0° and 16°. For the measurements at 0°, the transmission mode of the spectrometer [22] was used, where the proton beam passed through the spectrometer and stopped in a well-shielded Faraday cup located downstream of the spectrometer. For the measurements at 4°, a beam stopper was installed between the scattering chamber and the quadrupole magnet of the spectrometer. For measurements at angles larger than 4°, the beam was stopped by a beam stopper installed inside the scattering chamber.

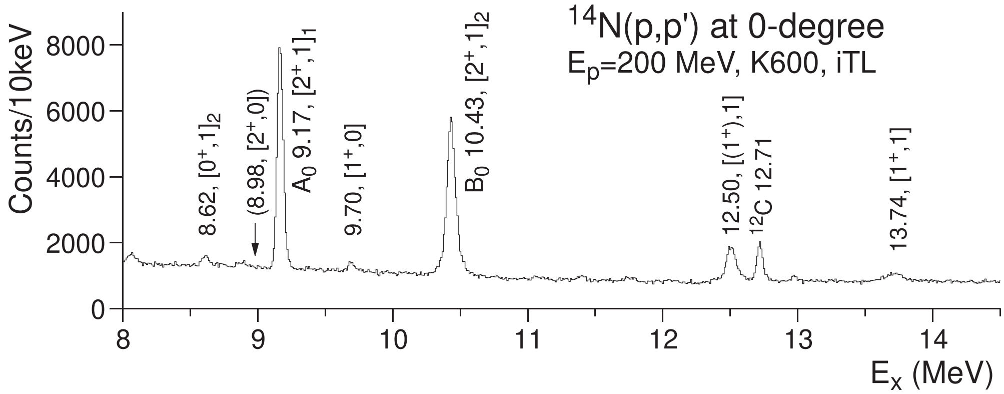

FIG. 2. The ^{14}N(p, p') spectrum at the spectrometer angle of 0°. The prominently excited states with $[J^\pi, T] = [2^+, 1]_1$ and $[2^+, 1]_2$ at 9.17 and 10.43 MeV are labeled as A_0 and B_0, respectively.

The scattered protons were detected by a pair of multiwire drift chambers (MWDCs) placed along the focal plane. Each MWDC consists of two sense wire planes, with one set of sense wires stretched vertically and the other set tilted at an angle of 50° with respect to the horizontal direction. This configuration allows the determination of both horizontal and vertical positions in the focal plane. From the position information in the MWDCs, the incident angles of the scattered protons were reconstructed. Two plastic scintillators behind the MWDCs were used for particle identification and to generate the timing signal.

Figure 2 shows the ^{14}N(p, p') spectrum obtained in the 0° measurement for the excitation energy (E_x) region between 8 and 14.5 MeV. An energy resolution of 54 keV (full width at half maximum) was achieved due to the dispersion-matched condition and software corrections for the defocusing effect in the focal plane caused by the kinematic recoil and magnetic field aberrations. The calibration of the E_x values was performed using the horizontal positions in the focal plane of the established states of ^{12}C and ^{14}N, after the necessary kinematic corrections. As can be seen in Fig. 2, the $[J^\pi, T] = [2^+, 1]_1$ and $[2^+, 1]_2$ states of interest at 9.17 and 10.43 MeV, respectively, are prominently excited. In this paper, these states are referred to as A_0 and B_0. For the B_0 state, a decay width of 31(5) keV was derived by peak-fit analysis [23]. This value is in good agreement with the value of 33(3) keV reported in Ref. [24].

As shown in Fig. 2, the 0^+, (1^+), and 1^+ states are also observed at 8.62 MeV, 12.50 MeV, and 13.74 MeV, respectively. Although the J^π values are not fully consistent, the candidates for their analogous states have been observed by the ^{14}N$(d, {}^2$He$)\,^{14}$C and ^{14}N$(^3$He$, t)\,^{14}$O measurements, as illustrated in Fig. 1 [14–16]. Therefore, we estimate that these states in ^{14}N have isospin $T = 1$ and are thus excited via the IV spin-$M1$ transitions.

IV. DATA ANALYSIS

A. Angular distributions of the A_0 and B_0 states

In the proportional relationship given by Eq. (7), a pure spin-isospin-flip process caused by the $\sigma\tau^0$ term of the nucleon-nucleon (NN) interaction without orbital angular momentum transfer (ΔL=0) is assumed. As mentioned above, the proportionality may be less accurate due to the incoherent contribution from the $\Delta L = 2$ component and the coherent contributions from the tensor ($T\tau$) part of the NN interaction. In addition, in the transitions from the ^{14}N ground state with $J^\pi = 1^+$ to the A_0 and B_0 states with 2^+, not only the ΔJ^π value of 1^+, but also 2^+ and 3^+ are allowed. The contributions from these non-$\sigma\tau^0$ processes are estimated by comparing the measured angular distributions with the distorted wave (DW) approximation calculations for the ^{14}N(p, p') reaction by using the DWBA07 computer code [25].

First, the dominance of the $\Delta J^\pi = 1^+$ component among the allowed ΔJ^π values of 1^+, 2^+, and 3^+ in the excitation of the A_0 and B_0 states is examined. Figures 3(a) and 3(b) compare the measured angular distributions of the A_0 and B_0 states with the DW calculations for the ΔJ^π values of 1^+, 2^+, and 3^+. The sums of these calculations are also shown. The

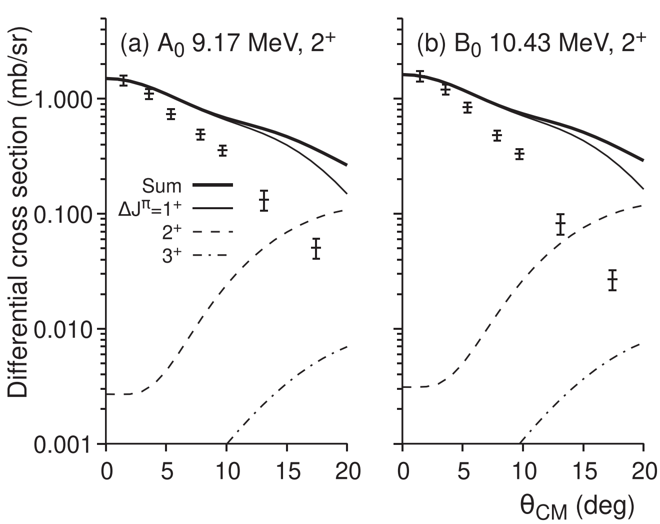

FIG. 3. The obtained angular distributions for (a) the 2^+ states at 9.17 (A_0) and (b) the 2^+ states at 10.43 MeV (B_0). Results of the DW calculations for the $\Delta J^\pi = 1^+$, 2^+, and 3^+ transitions and sum of these calculations are also shown. The calculated values are normalized by the factors determined for each state. For details of the calculations, see text.

calculated values are normalized by the factors determined for each state by comparing the measured cross sections and the sum of the calculated values at the forward scattering angles.

In the DW calculations, the Woods-Saxon optical potential parameters are obtained by interpolating the values for ^{12}C [26] and ^{16}O [27] at the incident proton energy of $E_p =$ 200 MeV. The transition densities for the excited states are derived from a shell-model (SM) calculation using the Nushell code [28]. Cohen-Kurath two-body matrix elements (CKME) [29] for the p-shell model space are applied. The Franey-Love (F-L) interaction at 210 MeV [30] is used as an effective NN interaction, with kinematic correction applied at $E_p =$ 200 MeV for target mass $A = 14$. Since the SM calculation predicts only one 2^+ state in the $E_x = 9 - 11$ MeV region, the same transition density is applied to both 2^+ states, A_0 and B_0.

Figures 3(a) and 3(b) show that the measured reaction cross sections of the A_0 and B_0 states exhibit similar forward-angle-dominant angular distributions. However, the calculated $\Delta J^\pi = 1^+$ angular distributions overestimate the measured values at larger scattering angles, suggesting that modifications are needed for the $\Delta J^\pi = 1^+$ calculations.

The calculated cross sections of $\Delta J^\pi = 2^+$ and 3^+ transitions exhibit larger values at larger scattering angles. Therefore, in both Figs. 3(a) and 3(b), even if the observed cross sections at larger scattering angles are solely due to $\Delta J^\pi = 2^+$ or 3^+ transitions, it is clear that these contributions are negligible at 0° compared to the $\Delta J^\pi = 1^+$ components.

For the same reason, it is also possible to study the amounts of the incoherent $\Delta L = 2$ contributions in the $\Delta J^\pi = 1^+$ transitions. As the angular distribution is primarily determined by the ΔL value, the angular distribution of the $\Delta L = 2$ component in the $\Delta J^\pi = 1^+$ transition is expected to be similar to that of the $\Delta J^\pi = 2^+$ transition, which is purely $\Delta L = 2$ (see Fig. 3). It can be concluded, therefore, that the $\Delta L = 2$ components in the $\Delta J^\pi = 1^+$ transitions in Figs. 3(a) and 3(b) are also negligible at 0° for the same reason as the $\Delta J^\pi = 2^+$ transitions.

The overestimation of the $\Delta J^\pi = 1^+$ calculations is examined as follows. In Figs. 4(a) and 4(b), the angular distributions for the A_0 and B_0 states are compared with the DW calculations using three types of effective interactions. The calculations for $\Delta J^\pi = 1^+$ using the full F-L interaction are shown by the solid lines, which are also shown in Fig. 3. The dashed and dot-dashed lines represent the calculations using only the central and tensor parts of the F-L interaction, respectively. The normalization factors used in Figs. 3(a) and 3(b) are also applied to the calculated values shown Figs. 4(a) and 4(b), respectively.

Both Figs. 4(a) and 4(b) demonstrate that the $\Delta J^\pi = 1^+$ calculations using the central part of the F-L interaction can reproduce the measured values well. On the other hand, the calculations using only the tensor part of the interaction become larger at larger angles, where the calculations using the full F-L interaction overestimate the measured values. According to these results, it appears that the transitions to the A_0 and B_0 states are mainly caused by the central part of the NN interaction, specifically the $\sigma\tau^0$ term. The overestimation by the DW calculations with the full F-L interaction can be attributed to the tensor part. It should be noted that the measured cross sections of the analogous $\Delta T_z = \pm 1$ transitions observed by the (^{3}He, t) and (d, ^{2}He) reactions are also overestimated by the DW calculations at larger scattering angles [15,16]. These results suggest that the contributions of the tensor part are also small in these transitions.

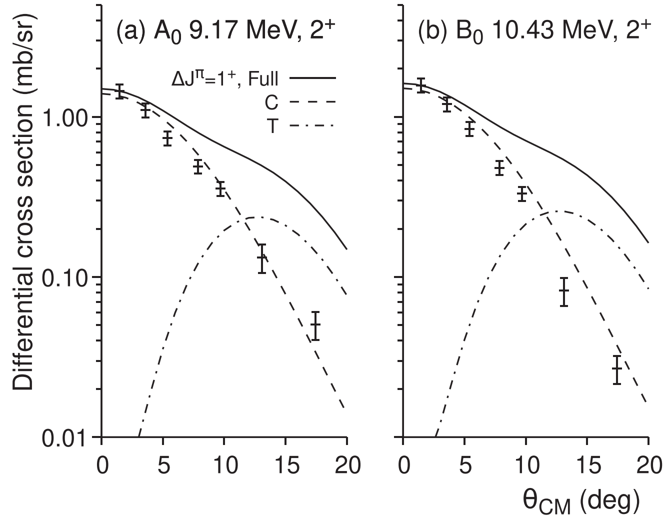

FIG. 4. The obtained angular distributions for (a) the 2^+ states at 9.17 (A_0) and (b) the 2^+ states at 10.43 MeV (B_0). Results of the DW calculations for the $\Delta J^\pi = 1^+$ transitions applying the full, central part (C), and tensor part (T) of the F-L interaction [30] are shown together. For details of the calculations, see text.

B. Angular distributions of the other states

As stated above, for the 0^+, (1^+), and 1^+ states at 8.62, 12.50, and 13.74 MeV, respectively, isospin $T = 1$ is inferred (see Figs. 1 and 2) and thus they are mainly excited via the IV spin-$M1$ transitions. By similar comparisons with the DW calculations performed for the A_0 and B_0 states, the contributions from the IV spin-$M1$ transitions in these states are examined.

In Figs. 5(a)–5(c), the measured angular distributions of these states are compared with the results of the DW calculations for $\Delta J^\pi = 1^+$. Details of the calculations are the same as for Fig. 4. The transition density for the 0^+ state at 8.62 MeV was estimated by the NORMOD computer code [31], since no 0^+ state appears around this energy region in the SM calculation.

In Fig. 5(a), the calculated values for the 0^+ state at 8.62 MeV with the central part of the F-L interaction show reasonable agreement with the measured values like the A_0 and B_0 states. On the other hand, in Figs. 5(b) and 5(c), the calculations for the states at 12.50 and 13.74 MeV with the full F-L interaction show better agreements than that with the central part of the interaction. These results suggest that, in the excitations of the 12.50- and 13.74-MeV states, the contributions from the noncentral part of the interaction are not negligible. From the ratios between the calculated cross sections for the 12.50- and 13.74-MeV states at 0° with the full F-L interaction and those with the central part, it is estimated that the ambiguities of the $B(\mathrm{GT}^0)$ values for the

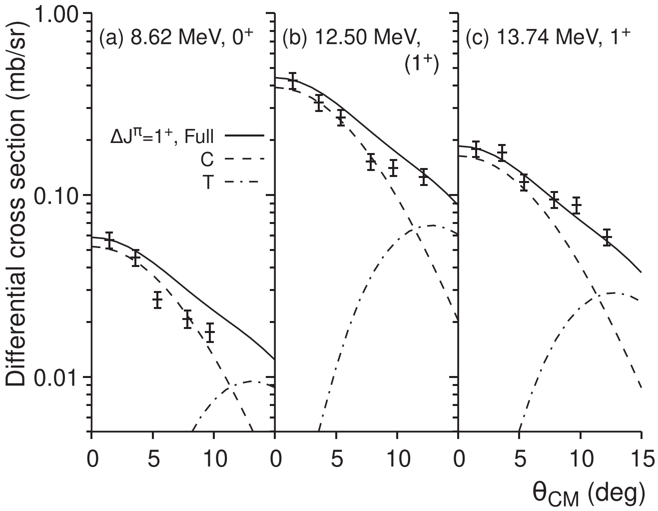

FIG. 5. The obtained angular distributions for (a) the 0^+ state at 8.62 MeV, (b) the (1^+) state at 12.50 MeV, and (c) the 1^+ state at 13.74 MeV. Results of the DW calculations for the $\Delta J^\pi = 1^+$ transitions applying the full, central part (C), and tensor part (T) of the F-L interaction [30] are shown together. For details of the calculations, see text.

12.50- and 13.74-MeV states due to the non-$\boldsymbol{\sigma}\tau^0$ transitions are ± 10 %.

C. Reduced transition strengths

The $B(\mathrm{GT}^0)$ values are derived using the proportional relationship given by Eq. (7). Assuming that the isospin asymmetry among the ^{14}C, ^{14}N, and ^{14}O nuclei occurs only between the $[J^\pi, T] = [2^+, 1]_1$ and $[2^+, 1]_2$ states, the sum of the $B(\mathrm{GT})$ values for these states in each nucleus should be conserved. Therefore, to determine the $B(\mathrm{GT}^0)$ calibration standard, we use the sum of the $B(\mathrm{GT}^-)$ values for the $[2^+, 1]_1$ and $[2^+, 1]_2$ states in ^{14}O, i.e., A_- and B_-, given in Ref. [16] as the sum of the $B(\mathrm{GT}^0)$ values for A_0 and B_0 in ^{14}N. The $B(\mathrm{GT}^+)$ values provided in Ref. [16] are also normalized in the same way using the $[2^+, 1]_1$ and $[2^+, 1]_2$ states in ^{14}C, i.e., A_+ and B_+.

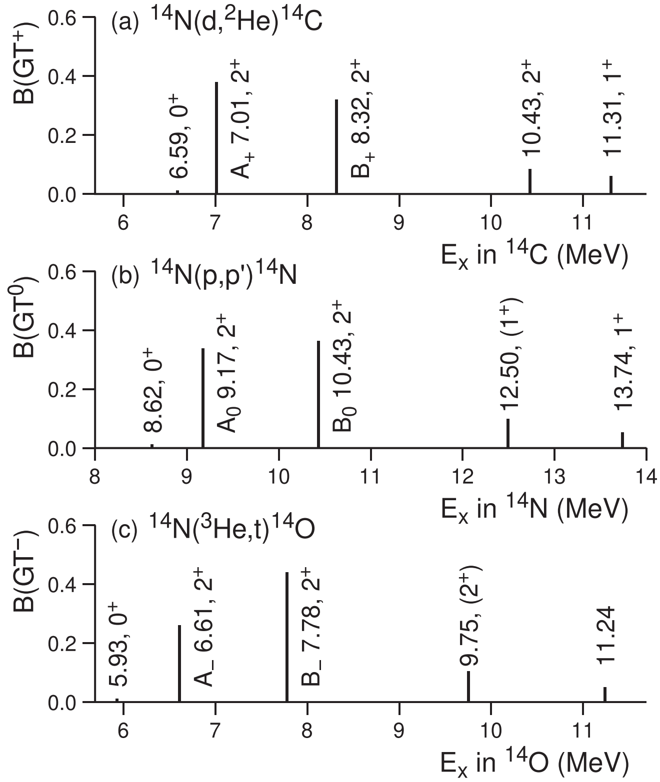

FIG. 6. The (a) $B(\mathrm{GT}^+)$, (b) $B(\mathrm{GT}^0)$, and (c) $B(\mathrm{GT}^-)$ values from the $^{14}\mathrm{N}(d, {}^2\mathrm{He})\,{}^{14}\mathrm{C}$ [16], $^{14}\mathrm{N}(p, p')$, and $^{14}\mathrm{N}({}^3\mathrm{He}, t)\,{}^{14}\mathrm{O}$ [16] data, respectively. The horizontal axes in (a) and (c) are shifted by 2.31 MeV, i.e., the excitation energy of the IAS in ^{14}N. Note that the $B(\mathrm{GT}^0)$ and $B(\mathrm{GT}^+)$ values are normalized by using the analogous $B(\mathrm{GT}^-)$ values.

The obtained $B(\mathrm{GT}^0)$ values and the analogous $B(\mathrm{GT}^\pm)$ values are summarized in Table I and Figs. 6(a)–6(c). Note that the E_x values of the excited states in ^{14}O are taken from Ref. [14]. In Fig. 6(b), the A_0 and B_0 states exhibit similar $B(\mathrm{GT}^0)$ values. On the other hand, in Fig. 6(a), the $B(\mathrm{GT}^+)$ value of the A_+ state is larger than that of the B_+ state, and in Fig. 6(c), the $B(\mathrm{GT}^-)$ value of the A_- state is smaller than that of the B_- state. In summary, the $B(\mathrm{GT})$ values in Figs. 6(a)–6(c) show seesaw-like systematic asymmetry.

TABLE I. The $B(\mathrm{GT}^+)$ values derived from the study via the $^{14}\mathrm{N}(d, {}^2\mathrm{He})\,{}^{14}\mathrm{C}$ reaction [16], the $B(\mathrm{GT}^0)$ values from the present $^{14}\mathrm{N}(p, p')$ reaction, and the $B(\mathrm{GT}^-)$ values from the $^{14}\mathrm{N}({}^3\mathrm{He}, t)\,{}^{14}\mathrm{O}$ reaction [16]. Note that the E_x values of the excited states in ^{14}O are taken from Ref. [14].

$^{14}\mathrm{N}(d, {}^2\mathrm{He})\,{}^{14}\mathrm{C}$			$^{14}\mathrm{N}(p, p')\,{}^{14}\mathrm{N}$			$^{14}\mathrm{N}({}^3\mathrm{He}, t)\,{}^{14}\mathrm{O}$		
E_x (MeV)	J^π	$B(\mathrm{GT}^+)$	E_x (MeV)	J^π	$B(\mathrm{GT}^0)$	E_x (MeV)	J^π	$B(\mathrm{GT}^-)$
6.589	0^+	0.012(2)	8.618	0^+	0.013(1)	5.931	0^+	0.011(1)
7.012 (A_+)	2^+	0.381(22)	9.172 (A_0)	2^+	0.338(18)	6.609 (A_-)	2^+	0.260(5)[a]
8.318 (B_+)	2^+	0.320(16)	10.432 (B_0)	2^+	0.363(20)	7.777 (B_-)	2^+	0.441(11)[a]
10.425	2^+	0.085(6)	12.495	(1^+)	0.098(11)	9.751	(2^+)	0.104(4)
11.306	1^+	0.062(5)	13.740	1^+	0.054(6)	11.239		0.051(2)
Total $B(\mathrm{GT})$		0.860(28)			0.866(30)			0.867(13)

[a] Used to determine the normalization standard value.

As shown in Table I and Fig. 6, the obtained $B(\mathrm{GT}^0)$ values for the 8.62, 12.50, and 13.74 MeV states agree within the uncertainties with those for the analogous states in ^{14}C and ^{14}O, although the transitions are relatively weak. This fact is reasonably consistent with the assumptions that the isospin asymmetry occurs only between the $[J^\pi, T] = [2^+, 1]_1$ and $[2^+, 1]_2$ states.

V. ISOSPIN ASYMMETRY

Applying a simple two-state model, we estimate the off-diagonal terms of the charge-dependent parts of the Hamiltonians $\langle H_C^+\rangle$ and $\langle H_C^-\rangle$ for ^{14}C and ^{14}O, respectively, which mix the $[J^\pi, T] = [2^+, 1]_1$ and $[2^+, 1]_2$ states in these nuclei, i.e., A_+ and B_+; A_- and B_-.

The A_0 and B_0 states in ^{14}N satisfy the relations

$$H_0\,|A_0\rangle = E_{A0}\,|A_0\rangle \tag{8}$$

and

$$H_0\,|B_0\rangle = E_{B0}\,|B_0\rangle, \tag{9}$$

where H_0 is the nuclear Hamiltonian for ^{14}N.

We write the Hamiltonians H^+ and H^- for ^{14}C and ^{14}O, respectively, as a sum of H_0 and the charge-dependent parts H_C^+ and H_C^-,

$$H^\pm = H_0 + H_C^\pm. \tag{10}$$

In this two-state model, we assume that the A_+ and B_+ states in ^{14}C are written as a mixture of A_0 and B_0 states as

$$|A_+\rangle = \alpha_+\,|A_0\rangle + \beta_+\,|B_0\rangle, \tag{11}$$

$$|B_+\rangle = -\beta_+\,|A_0\rangle + \alpha_+\,|B_0\rangle. \tag{12}$$

Similarly, the A_- and B_- states in ^{14}O are written as

$$|A_-\rangle = \alpha_-\,|A_0\rangle + \beta_-\,|B_0\rangle, \tag{13}$$

$$|B_-\rangle = -\beta_-\,|A_0\rangle + \alpha_-\,|B_0\rangle, \tag{14}$$

where $\alpha_\pm^2 + \beta_\pm^2 = 1$. Under our assumption that the isospin asymmetry is a minor effect, $\beta_\pm^2 \ll 1$ is expected. Note that, the sums of the $B(\mathrm{GT}^X)$ values for the A_X and B_X states are conserved, where X denotes 0, +, and −.

For ^{14}C and ^{14}O, $A_\pm$ and $B_\pm$ satisfy

$$H^\pm\,|A_\pm\rangle = E_{A\pm}\,|A_\pm\rangle, \tag{15}$$

$$H^\pm\,|B_\pm\rangle = E_{B\pm}\,|B_\pm\rangle. \tag{16}$$

Using these relations, the off-diagonal matrix element of $H_C^\pm$ connecting A_0 and B_0, $\langle H_C^\pm\rangle$, can be written as

$$\begin{aligned}\langle H_C^\pm\rangle &= \langle A_0|\,H_C^\pm\,|B_0\rangle\\ &= \alpha_\pm\beta_\pm(E_{A\pm} - E_{B\pm}).\end{aligned} \tag{17}$$

Using the $B(\mathrm{GT}^0)$ and $B(\mathrm{GT}^+)$ values given in Table I, values for α_+ and β_+ of 0.998 and 0.061 are respectively obtained. Similarly using the $B(\mathrm{GT}^0)$ and $B(\mathrm{GT}^-)$ values, we obtain α_- and β_- values of 0.994 and −0.113, respectively. Further applying Eq. (17), the off-diagonal terms of the charge-dependent Hamiltonians are estimated to be $\langle H_C^+\rangle = -80(40)$ keV for ^{14}C and $\langle H_C^-\rangle = +130(30)$ keV for ^{14}O. The obtained $\langle H_C^\pm\rangle$ values show a roughly proportional relationship with the $T_z = (N - Z)/2$ values for the respective nuclei, which can be written as

$$\langle H_C\rangle = kT_z, \tag{18}$$

where $k = -105$ keV.

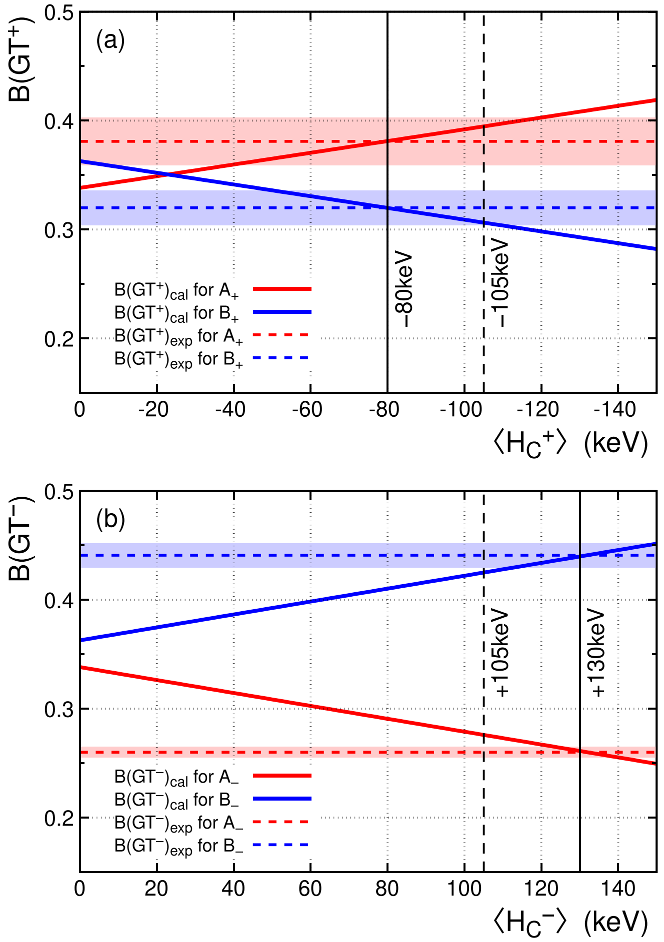

FIG. 7. The (a) $B(\mathrm{GT}^+)$ and (b) $B(\mathrm{GT}^-)$ values for the $A_\pm$ and $B_\pm$ states as functions of the $\langle H_C^+\rangle$ and $\langle H_C^-\rangle$ values, respectively, which are denoted by $B(\mathrm{GT})_{\mathrm{cal}}$. The red and blue horizontal bands show the measured $B(\mathrm{GT}^\pm)$ values for these states, which are denoted by $B(\mathrm{GT})_{\mathrm{exp}}$. Note that the horizontal axis in (a) is reversed. The vertical solid lines at $\langle H_C^+\rangle = -80$ keV and $\langle H_C^-\rangle = +130$ keV indicate the obtained $\langle H_C^\pm\rangle$ values from the present analysis. The $\langle H_C^\pm\rangle$ values of ±105 keV assuming the proportional relationship with T_z is indicated by the dashed lines.

VI. DISCUSSION

In Figs. 7(a) and 7(b), the $B(\mathrm{GT}^+)$ and $B(\mathrm{GT}^-)$ values for the A_+ and B_+; A_- and B_- states as functions of the $\langle H_C^+\rangle$ and $\langle H_C^-\rangle$ values are compared with the measured $B(\mathrm{GT}^\pm)$ values, respectively. The former and the latter are denoted by $B(\mathrm{GT}^\pm)_{\mathrm{cal}}$ and $B(\mathrm{GT}^\pm)_{\mathrm{exp}}$, respectively. At $\langle H_C^+\rangle = -80$ keV in Fig. 7(a) and $\langle H_C^-\rangle = +130$ keV in Fig. 7(b), the $B(\mathrm{GT}^\pm)_{\mathrm{cal}}$

values agree with the measured values. As can be seen from Fig. 7(a), the relatively larger uncertainty of the obtained $\langle H_C^+ \rangle$ value is due to the uncertainties of the measured $B(\mathrm{GT}^+)$ values.

From the proportional relationship given by Eq. (18) between $\langle H_C^\pm \rangle$ and T_z, we obtain $\langle H_C^+ \rangle = -105$ keV for ^{14}C with $T_z = +1$ and $\langle H_C^- \rangle = +105$ keV for ^{14}O with $T_z = -1$. Note that, both values are within the uncertainties of the obtained values, $\langle H_C^+ \rangle = -80(40)$ keV and $\langle H_C^- \rangle = +130(30)$ keV. As indicated by the dashed line in Fig. 7(a), at $\langle H_C^+ \rangle = -105$ keV, the $B(\mathrm{GT}^+)_{\mathrm{cal}}$ values agree with the measured $B(\mathrm{GT}^+)_{\mathrm{exp}}$ values within the uncertainties. On the other hand, although the $B(\mathrm{GT}^-)_{\mathrm{cal}}$ values at $\langle H_C^- \rangle = +105$ keV could not reproduce the measured values within the uncertainties, the differences are less than 0.02 [see Fig. 7(b)], which correspond to $+6\%$ and -4% for the A_- and B_- states, respectively. These facts suggest that the proportional relationship given by Eq. (18) between $\langle H_C^\pm \rangle$ and T_z is reasonably valid.

The empirical [32] and theoretical [33–35] studies suggest that the $[J^\pi, T] = [0^+, 1]_2$ and $[2^+, 1]_2$ states in ^{14}C have cluster structures. Note that the latter corresponds to the B_+ state. As stated above, the SM calculation using the CKME interaction could not reproduce their analogous states in ^{14}N. From the analogous relationships with the B_+ state, similar cluster structures are expected also for the B_0 and B_- states in ^{14}N and ^{14}O, respectively. Assuming the cluster structures consist of three α-particles and two valence nucleons, the valence nucleons in ^{14}C, ^{14}N, and ^{14}O are two neutrons, one proton and one neutron, and two protons, respectively. The isospin asymmetry discussed in this paper may be due to the different contributions from the Coulomb interaction between the valence nucleons and the α-particles, which can cause different mixtures with the neighboring $[2^+, 1]_1$ states, A_+, A_0, and A_-.

In Ref. [36], a theoretical discussion of possible isospin mixing in ^{14}N between the $[J^\pi, T] = [2^+, 1]_1$ state at 9.17 MeV, i.e., the A_0 state, and the nearby $[2^+, 0]$ state at 8.98 MeV is given. If such isospin mixing occurs, then the excitation of the 8.98-MeV state can have contributions not only from the IS spin-$M1$, but also from the IV spin-$M1$ transition, which is usually much stronger than the IS spin-$M1$ transition [1,6]. However, there is no clear indication of the 8.98-MeV state in Fig. 2.

VII. SUMMARY

The ^{14}N(p, p') measurement was performed at $E_p = 200$ MeV with the spectrometer angles of 0°–16° using the K600 magnetic spectrometer at iThemba LABS, South Africa. The reduced transition strengths $B(\mathrm{GT}^0)$ were derived for the observed IV spin-$M1$ transitions. By comparing the obtained $B(\mathrm{GT}^0)$ values for the $[J^\pi, T] = [2^+, 1]_1$ and $[2^+, 1]_2$ states in ^{14}N with those for the analogous states in ^{14}C and ^{14}O, isospin asymmetry among these nuclei was investigated. As shown in Fig. 6, the $B(\mathrm{GT})$ values for these states in ^{14}C, ^{14}N, and ^{14}O display systematic asymmetry. From the $B(\mathrm{GT}^0)$ and $B(\mathrm{GT}^+)$ values, the $\langle H_C^+ \rangle$ value of $-80(40)$ keV was obtained for ^{14}C. On the other hand, from the $B(\mathrm{GT}^0)$ and $B(\mathrm{GT}^-)$ values, a larger $\langle H_C^- \rangle$ value of $+130(30)$ keV has been derived for ^{14}O. The $\langle H_C^\pm \rangle$ values suggest a roughly proportional relationship with the T_z values of residual nuclei, ^{14}C and ^{14}O.

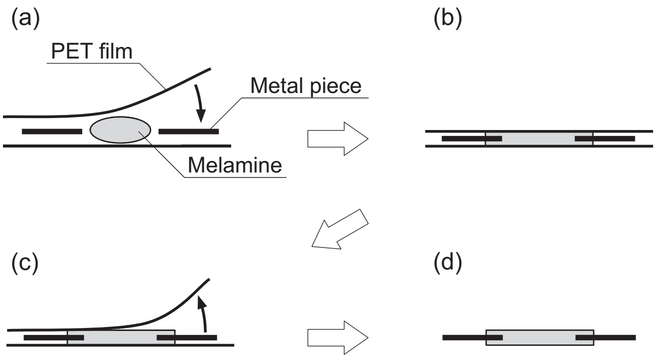

FIG. 8. Procedure to form the thin melamine resin target: (a) The melamine solution is sandwiched by the PET films together with the metal piece. (b) The solution is stretched by its own surface tension during the polymerization process. (c) The PET films are peeled off after the polymerization. (d) The melamine resin is fixed on the metal piece, by which it can be mounted on the target frame.

ACKNOWLEDGMENTS

We thank the accelerator group of iThemba LABS for providing a high-quality proton beam. H.F. thanks S. Sasaki for valuable discussions in the evaluation of the research results. Y.F. acknowledges the support of MEXT, Japan under Grant No. 15K05104. This work is based on research supported in part by the National Research Foundation of South Africa (Grant No. 85509).

APPENDIX: THIN MELAMINE TARGET

This section explains the polymerization procedure of melamine, which was utilized as a solid and self-supporting ^{14}N targets in the ^{14}N(p, p') experiment.

Heat treatment of melamine and formaldehyde was performed in a formalin solution at a temperatures of 80°C for 30 min. The molar ratio of formaldehyde to melamine was 2:1. The pH value of the solution was kept between 10 and 12 by adding ammonia water. Sodium hydroxide was not used to optimize the pH, due to the potential degradation of the (p, p') spectrum by the odd mass ^{23}Na nucleus which has a high level density.

As depicted in Figs. 8(a) and 8(b), two polyethylene terephthalate (PET) films were used to sandwich a high-viscosity melamine solution and a metal piece that was used to mount the melamine target to the target frame. A 200-μm-thick stainless steel plate with an oval hole (22 mm × 8 mm) and a 10-μm-thick aluminium foil with a round hole of 12–16 mm diameter were used as the metal pieces. The PET films covering the hole on either side of the metal ensures the melamine solution filling the hole polymerizes with flat surfaces while also spreading a thin layer over the metal [see Fig. 8(b)]. After the polymerization, the melamine resin adhered to the metal piece, and the PET films were removed [see Figs. 8(c) and 8(d)]. The production of melamine resin with an areal density of $\sim$10 mg/cm^2 could be realized using alminium foil as the metal to support the target.

[1] Y. Fujita, B. Rubio, and W. Gelletly, Prog. Part. Nucl. Phys. **66**, 549 (2011), and references therein.
[2] P. von Neumann-Cosel and A. Tamii, Eur. Phys. J. A **55**, 110 (2019), and references therein.
[3] J. Rapaport and E. Sugarbaker, Annu. Rev. Nucl. Part. Sci. **44**, 109 (1994).
[4] C. D. Goodman, C. A. Goulding, M. B. Greenfield, J. Rapaport, D. E. Bainum, C. C. Foster, W. G. Love, and F. Petrovich, Phys. Rev. Lett. **44**, 1755 (1980).
[5] T. N. Taddeucci, C. A. Goulding, T. A. Carey, R. C. Byrd, C. D. Goodman, C. Gaarde, J. Larsen, D. J. Horen, J. Rapaport, and E. Sugarbaker, Nucl. Phys. A **469**, 125 (1987), and references therein.
[6] H. Matsubara, A. Tamii, H. Nakada, T. Adachi, J. Carter, M. Dozono, H. Fujita, K. Fujita, Y. Fujita, K. Hatanaka, W. Horiuchi, M. Itoh, T. Kawabata, S. Kuroita, Y. Maeda, P. Navrátil, P. von Neumann-Cosel, R. Neveling, H. Okamura, L. Popescu, I. Poltoratska, A. Richter *et al.*, Phys. Rev. Lett. **115**, 102501 (2015).
[7] C. Djalali, G. M. Crawley, B. A. Brown, V. Rotberg, G. Caskey, A. Galonsky, N. Marty, M. Morlet, and A. Willis, Phys. Rev. C **35**, 1201 (1987).
[8] G. M. Crawley, C. Djalali, N. Marty, M. Morlet, A. Willis, N. Anantaraman, B. A. Brown, and A. Galonsky, Phys. Rev. C **39**, 311 (1989).
[9] H. Fujita, Y. Fujita, T. Adachi, H. Akimune, N. T. Botha, K. Hatanaka, H. Matsubara, K. Nakanishi, R. Neveling, A. Okamoto, Y. Sakemi, T. Shima, Y. Shimizu, F. D. Smit, T. Suzuki, A. Tamii, and M. Yosoi, Phys. Rev. C **88**, 054329 (2013).
[10] T. G. Dzubay, R. Sherr, F. D. Becchetti, Jr., D. Dehnhard, Nucl. Phys. A **142**, 488 (1970).
[11] H. Orihara, K. Ogawa, T. Murakami, S. Nishihara, T. Nakagawa, and K. Maeda, Nucl. Phys. A **403**, 317 (1983).
[12] Y. Fujita, Y. Shimbara, T. Adachi, G. P. A. Berg, B. A. Brown, H. Fujita, K. Hatanaka, J. Kamiya, K. Nakanishi, Y. Sakemi, S. Sasaki, Y. Shimizu, Y. Tameshige, M. Uchida, T. Wakasa, and M. Yosoi, Phys. Rev. C **70**, 054311 (2004).
[13] Y. Shimbara, Y. Fujita, T. Adachi, G. P. A. Berg, H. Fujimura, H. Fujita, K. Fujita, K. Hara, K. Y. Hara, K. Hatanaka, J. Kamiya, K. Katori, T. Kawabata, K. Nakanishi, G. Martìnez-Pinedo, N. Sakamoto, Y. Sakemi, Y. Shimizu, Y. Tameshige, M. Uchida, M. Yoshifuku *et al.*, Phys. Rev. C **86**, 024312 (2012).
[14] A. Negret, T. Adachi, G. P. A. Berg, P. von Brentano, H. Fraiquin, D. De Frenne, H. Fujita, K. Fujita, Y. Fujita, K. Hatanaka, K. Jacobs, K. Nakanishi, L. Popescu, Y. Sakemi, Y. Shimbara, Y. Shimizu, Y. Tameshige, A. Tamii, M. Uchida, and M. Yosoi, Phys. Rev. C **71**, 047303 (2005).
[15] A. Negret, T. Adachi, B. R. Barett, C. Bäumer, A. M. van den Berg, G. P. A. Berg, P. von Brentano, D. Frekers, D. De Frenne, H. Fujita, K. Fujita, Y. Fujita, E.-W. Grewe, P. Haefner, M. N. Harakeh, K. Hatanaka, K. Heyde, M. Hunyadi, E. Jacobs, Y. Kalmykov, A. Korff, K. Nakanishi, P. Navrátil *et al.*, Phys. Rev. Lett. **97**, 062502 (2006).
[16] A. Negret, Ph.D. thesis, Faculteit Wetenschappen, Universiteit Gent, 2005.
[17] I. S. Towner, Phys. Rep. **155**, 263 (1987).
[18] S. Giraud, J. C. Zamora, R. G. T. Zegers, D. Bazin, Y. Ayyad, S. Bacca, S. Beceiro-Novo, B. A. Brown, A. Carls, J. Chen, M. Cortesi, M. DeNudt, G. Hagen, C. Hultquist, C. Maher, W. Mittig, F. Ndayisabye, S. Noji, S. J. Novario, J. Pereira *et al.*, Phys. Rev. Lett. **130**, 232301 (2023).
[19] R. G. T. Zegers, H. Akimune, S. M. Austin, D. Bazin, A. M. van den Berg, G. P. A. Berg, B. A. Brown, J. Brown, A. L. Cole, I. Daito, Y. Fujita, M. Fujiwara, S. Galès, M. N. Harakeh, H. Hashimoto, R. Hayami, G. W. Hitt, M. E. Howard, M. Itoh, J. Jänecke, T. Kawabata, K. Kawase, M. Kinoshita *et al.*, Phys. Rev. C **74**, 024309 (2006).
[20] Y. Fujita, K. Hatanaka, G. P. A. Berg, K. Hosono, N. Matsuoka, S. Morinobu, T. Noro, M. Sato, K. Tamura, and H. Ueno, Nucl. Instrum. Methods B **126**, 274 (1997).
[21] H. Fujita, Y. Fujita, G. P. A. Berg, A. D. Bacher, C. C. Foster, K. Hara, K. Hatanaka, T. Kawabata, T. Noro, H. Sakaguchi, Y. Shimbara, T. Shinada, E. J. Stephenson, H. Ueno, and M. Yosoi, Nucl. Instrum. Methods A **484**, 17 (2002).
[22] R. Neveling, H. Fujita, F. D. Smit, T. Adachi, G. P. A. Berg, E. Z. Buthelezi, J. Carter, J. L. Conradie, M. Couder, R. W. Fearick, S. V. Förtsch, D. T. Fourie, Y. Fujita, J. Görres, K. Hatanaka, M. Jingo, A. M. Krumbholz, C. O. Kureba, J. P. Mira, S. H. T. Murray, P. von Neumann-Cosel, S. O'Brien *et al.*, Nucl. Instrum. Methods A **654**, 29 (2011).
[23] H. Fujita *et al.*, RCNP (Osaka University) Annual Report (2010).
[24] F. Ajzenberg-selove, Nucl. Phys. A **523**, 1 (1991), and references therein.
[25] J. Raynal, DWBA07, a DWBA computer code, NEA data bank NEA-1209, https://www.oecd-nea.org/tools/abstract/detail/nea-1209/.
[26] H. O. Meyer, P. Schwandt, W. W. Jacobs, and J. R. Hall, Phys. Rev. C **27**, 459 (1983).
[27] C. W. Glover, P. Schwandt, H. O. Meyer, W. W. Jacobs, J. R. Hall, M. D. Kaitchuck, and R. P. DeVito, IUCF (Indiana University, 1982), Annual Report, 9.
[28] B. A. Brown, A. Etchegoyen, N. S. Godwin, W. D. M. Rae, W. A. Richter, W. E. Ormand, E. K. Warburton, J. S. Winfield, L. Zhao, and C. H. Zimmerman, NSCL report 524.
[29] S. Cohen and D. Kurath, Nucl. Phys. **73**, 1 (1965).
[30] M. A. Franey and W. G. Love, Phys. Rev. C **31**, 488 (1985).
[31] S. Y. van der Werf, computer program NORMOD (unpublished).
[32] W. von Oertzen, H. G. Bohlen, M. Milin, T. Kokalova, S. Thummerer, A. Tumino, R. Kalpakchieva, T. N. Massey, Y. Eisermann, G. Graw, T. Faestermann, R. Hertenberger, and H.-F. Wirth, Eur. Phys. J. A **21**, 193 (2004).
[33] N. Itagaki, T. Otsuka, K. Ikeda, and S. Okabe, Phys. Rev. Lett. **92**, 142501 (2004).
[34] T. Suhara and Y. Kanada-En'yo, Phys. Rev. C **82**, 044301 (2010).
[35] Y. Kanada-En'yo and T. Suhara, Phys. Rev. C **89**, 044313 (2014).
[36] H. T. Fortune, Phys. Rev. C **95**, 024325 (2017).